Aerodynamic Parameter Estimation Using Reconstructed Turbulence Measurements

Jared A. Grauer*
NASA Langley Research Center, Hampton, Virginia, 23681

A classical method for reconstructing atmospheric turbulence from onboard measurements of airdata and inertial sensors was improved. The reconstructed turbulence was included in a system identification analysis to estimate nondimensional stability and control derivatives in a longitudinal short period model using the maximum likelihood equation-error method with Fourier transform data. Practical aspects of the approach are discussed, such as reconstruction accuracy, data collinearity, model structure, and real-time estimation. Results using simulation and flight test data for a subscale airplane indicated that accurate turbulence reconstructions and parameter estimates could be obtained from maneuvering flight in high levels of turbulence.

I. Nomenclature

a_x, a_y, a_z	=	accelerometer measurements, g
C_a	=	nondimensional aerodynamic coefficient for $a = Z$ or m
cov	=	covariance operator
$\bar{c}$	=	mean aerodynamic chord, ft
$\mathcal{F}$	=	Fourier transform operator
g	=	gravitational acceleration, ft/s^2
I_{xx}, I_{yy}, I_{zz}, I_{xz}	=	moments and product of inertia, slug-ft^2
j	=	imaginary number, = $\sqrt{-1}$
M_T	=	pitching moment from propulsion, ft-lbf
m	=	aircraft mass, slug
p, q, r	=	angular rates, rad/s
$\bar{q}$	=	dynamic pressure, lbf/ft^2
$\Re$	=	real part
S	=	wing reference area, ft^2
t	=	time, s
u, v, w	=	translational velocities, ft/s
V	=	true airspeed, ft/s
x, y, z	=	body-axis coordinates, ft
α	=	angle of attack, rad
β	=	sideslip angle, rad
Δ	=	perturbation
δ_e	=	elevator deflection, rad
ϕ, θ, ψ	=	Euler angles, rad
$\lvert . \rvert$	=	magnitude, dB
$\angle$	=	phase angle, deg
†	=	complex conjugate transpose
$\hat{}$	=	estimated value
$^{-1}$	=	matrix inverse
^{T}	=	matrix transpose
$\dot{}$	=	time derivative

*Research Engineer, Dynamic Systems and Control Branch, MS 308, Associate Fellow AIAA.

II. Introduction

Atmospheric turbulence is often present during flight tests. Because turbulence affects the motion of the aircraft but is not directly measured, the accuracy of most system identification analyses degrades when turbulence levels are significant. For example, the maximum likelihood output-error method using time-domain data [1], assumes all inputs are accurately measured. When significant turbulence is present, matches to measured output data become poor and parameter estimates incur biases and large uncertainties.

The most common and simple approach to mitigate the adverse effects of turbulence on system identification is to only conduct flight tests in calm air when the effects of turbulence are negligible. However, this practice can result in schedule delays in testing and additional costs. In cases where the flight data cannot be repeated, such as during accident investigations or expensive flight test experiments, the effects of turbulence can lead to inaccurate estimation results and incorrect conclusions. If testing in turbulence cannot be avoided, an effective approach is to increase amplitudes of excitation inputs to reduce the effects of turbulence [2], although care must be taken to keep the response small enough to maintain modeling assumptions and to stay within maneuver load limits.

Another approach is to alter the analysis method to account for the turbulence. In the maximum likelihood filter-error method [1, 3] and nonlinear state estimation [4], turbulence can be considered process noise or an additional state driven by white noise. These methods can be difficult to use because of increased complexity, convergence problems, and unrealistic assumptions about turbulence. In contrast, the maximum likelihood equation-error method [2, 3] is a simpler approach that allows for process noise on the aircraft model and is routinely used for aircraft system identification. Equation error was used in Ref. [2] to obtain satisfactory estimates of stability and control derivatives for flight in turbulence. References [5, 6] further investigated sources of error and colored noise when using this method.

This paper presents a different approach in which turbulence was reconstructed from other measurements and included as a known input in the parameter estimation. The reconstruction was based on a classical technique that combines measured airdata and inertial information, but was improved in this work by retaining the full nonlinear equations and using frequency-domain data to remove bias errors, increase signal-to-noise ratios, and enable real-time modeling. The approach was demonstrated using simulation and flight test data for a subscale airplane to estimate stability and control derivatives in the short-period model using the equation-error method with Fourier-transform data. The main contributions of this paper are the improved turbulence reconstruction and the discussion surrounding its application to aerodynamic parameter estimation.

The organization of this paper is as follows. Section III describes the mathematical representation of the turbulence. Section IV discusses the aerodynamic model and the short period dynamics considering turbulence. Section V summarizes parameter estimation in the frequency domain using equation error. Section VI presents the method for turbulence reconstruction. Section VII describes the T-2 subscale airplane, and results obtained using simulation data and flight test data are discussed in Section VIII. Further discussions and conclusions are given in Section IX. The analysis used routines from the MATLAB®-based software package called System IDentification Programs for AirCraft, or SIDPAC [7], which is associated with Ref. [3].

III. Turbulence Definition

The terms turbulence, gust, and winds are used interchangeably in this paper to refer to any motion of the atmosphere relative to the Earth-fixed reference frame. The development is focused on the vertical and apparent pitching components of turbulence, but the approach is similar for other components, as discussion later in Section VI.

Several sign conventions are used in the literature to define turbulence. The convention used in Refs. [8–10] is followed in this paper, in which the vertical gust component w_g is positive when the wind moves downward around the aircraft, in the direction of the positive z body axis. With regard to the modeled aerodynamics, this motion is equivalent to the airplane moving upwards with an equal velocity through a still atmosphere. Small $w_g > 0$ therefore create the approximate gust angle of attack

$$\alpha_g \simeq -\frac{w_g}{u} \tag{1}$$

As the aircraft traverses the turbulence field, an apparent rotational motion of the atmosphere relative to the aircraft manifests from the gust gradient. For large spatial wavelengths of the turbulence relative to the aircraft size, and for small changes in forward speed, the resulting pitch rate gust is approximated as

$$q_g = -\frac{\partial w_g}{\partial x} = -\frac{\partial w_g/\partial t}{\partial x/\partial t} \simeq -\frac{\dot{w}_g}{u} \simeq \dot{\alpha}_g \tag{2}$$

This definition of q_g uses a sign convention consistent with α_g.

IV. Postulated Flight Dynamics Model

The aerodynamic forces and moments are represented as first-order Taylor series expansions about a reference flight condition. The body-axis velocity components of the aircraft relative to the moving atmosphere are used in these expansions to account for turbulence. Perturbations to the nondimensional aerodynamic coefficients involving short-period motions are postulated using body-axis parameters [8] as

$$\Delta C_a = C_{a_w}\left(\Delta w - \Delta w_g\right) + C_{a_{\dot{w}}}\left(\dot{w} - \dot{w}_g\right)\frac{\bar{c}}{2u} + C_{a_q}\left(q - q_g\right)\frac{\bar{c}}{2u} + C_{a_{\delta_e}}\Delta\delta_e \tag{3}$$

for $a = Z$ or m, which pertain to the vertical force coefficient or pitching moment coefficient. The aircraft mass, geometry, airspeed, and dynamic pressure are assumed to be constant. By substituting Eqs. (1) and (2) into (3), the aerodynamic coefficients can alternatively be expressed for low angles of attack in the stability axes [11] as

$$\Delta C_a = C_{a_\alpha}\left(\Delta\alpha + \Delta\alpha_g\right) + C_{a_{\dot{\alpha}}}\left(\dot{\alpha} + \dot{\alpha}_g\right)\frac{\bar{c}}{2V} + C_{a_q}\left(q - \dot{\alpha}_g\right)\frac{\bar{c}}{2V} + C_{a_{\delta_e}}\Delta\delta_e \tag{4}$$

Under these assumptions, the linearized equations of motion for the short-period approximation are

$$\dot{\alpha} = q + \frac{\bar{q}S}{mV}\Delta C_Z \tag{5a}$$

$$\dot{q} = \frac{\bar{q}S\bar{c}}{I_{yy}}\Delta C_m \tag{5b}$$

$$\dot{\theta} = q \tag{5c}$$

These equations can be expanded using Eq. (4) and assembled into the linear state-space format

$$\begin{bmatrix} \dot{\alpha} \\ \dot{q} \\ \dot{\theta} \end{bmatrix} = \begin{bmatrix} \frac{c_2}{c_3}C_{Z_\alpha} & \frac{1+c_1c_2C_{Z_q}}{c_3} & 0 \\ c_4C'_{m_\alpha} & c_1c_4C'_{m_q} & 0 \\ 0 & 1 & 0 \end{bmatrix}\begin{bmatrix} \Delta\alpha \\ q \\ \Delta\theta \end{bmatrix} + \begin{bmatrix} \frac{c_2}{c_3}C_{Z_{\delta_e}} & \frac{c_2}{c_3}C_{Z_\alpha} & \frac{c_1c_2}{c_3}\left(C_{Z_{\dot{\alpha}}} - C_{Z_q}\right) \\ c_4C'_{m_{\delta_e}} & c_4C'_{m_\alpha} & c_1c_4C^\circ_{m_q} \\ 0 & 0 & 0 \end{bmatrix}\begin{bmatrix} \Delta\delta_e \\ \Delta\alpha_g \\ \dot{\alpha}_g \end{bmatrix} \tag{6}$$

where, for convenience, the constants were defined

$$c_1 = \frac{\bar{c}}{2V} \tag{7a}$$

$$c_2 = \frac{\bar{q}S}{mV} \tag{7b}$$

$$c_3 = 1 - c_1c_2C_{Z_{\dot{\alpha}}} \tag{7c}$$

$$c_4 = \frac{\bar{q}S\bar{c}}{I_{yy}} \tag{7d}$$

$$c_5 = c_6\left(1 + \frac{c_1c_2}{c_3}C_{Z_{\dot{\alpha}}}\right) \tag{7e}$$

$$c_6 = \frac{\bar{q}S}{mg} \tag{7f}$$

and the lumped moment derivatives were defined

$$C'_{m_\alpha} = C_{m_\alpha} + \frac{c_1c_2}{c_3}C_{Z_\alpha}C_{m_{\dot{\alpha}}} \tag{8a}$$

$$C'_{m_q} = C_{m_q} + \frac{1 + c_1c_2C_{Z_q}}{c_3}C_{m_{\dot{\alpha}}} \tag{8b}$$

$$C'_{m_\delta} = C_{m_\delta} + \frac{c_1c_2}{c_3}C_{Z_\delta}C_{m_{\dot{\alpha}}} \tag{8c}$$

$$C^\circ_{m_q} = \left(C_{m_{\dot{\alpha}}} - C_{m_q}\right) + \frac{c_1c_2}{c_3}\left(C_{Z_{\dot{\alpha}}} - C_{Z_q}\right)C_{m_{\dot{\alpha}}} \tag{8d}$$

The model states are the aircraft angle of attack at the center of mass and the pitch rate. The inputs are the elevator deflection, gust angle of attack, and gust angle of attack rate. This model is similar to a conventional short period approximation but includes the added effects of the angle of attack gusts and rates. Formulating the gusts as inputs, rather as states such as in Ref. [11], is more convenient for parameter estimation using reconstructed turbulence because an additional state equation for the turbulence does not have to be modeled.

The state-space model is completed by the linearized output equations for the angle of attack vane, pitch rate gyroscope, vertical accelerometer at the center of mass, and Euler pitch angle

$$\begin{bmatrix} \Delta\alpha_v \\ q \\ \Delta a_z \\ \Delta\theta \end{bmatrix} = \begin{bmatrix} 1 & -x_\alpha/V & 0 \\ 0 & 1 & 0 \\ c_5 C_{Z_\alpha} & \left(\frac{c_1 c_6}{c_3}\frac{C_{Z_{\dot\alpha}}}{C_{Z_q}} + c_1 c_5\right) C_{Z_q} & 0 \\ 0 & 0 & 1 \end{bmatrix} \begin{bmatrix} \Delta\alpha \\ q \\ \Delta\theta \end{bmatrix} + \begin{bmatrix} 0 & 1 & 0 \\ 0 & 0 & 0 \\ c_5 C_{Z_{\delta_e}} & c_5 C_{Z_\alpha} & c_1 c_5 \left(C_{Z_{\dot\alpha}} - C_{Z_q}\right) \\ 0 & 0 & 0 \end{bmatrix} \begin{bmatrix} \Delta\delta_e \\ \Delta\alpha_g \\ \dot\alpha_g \end{bmatrix} \tag{9}$$

where x_α is the location of the angle of attack vane relative to the aircraft center of mass along the x body axis.

V. Parameter Estimation in the Frequency Domain

This section briefly summarizes the approach for estimating the nondimensional stability and control derivatives in Eq. (4) from measured data. Fourier transforms are first reviewed, followed by the equation-error method for parameter estimation. For more information, see Ref. [3].

A. Fourier Transform

The analytical tool for transforming measured data from the time domain into the frequency domain is the finite Fourier transform

$$x(j\omega_k) = \mathcal{F}[x(t)] = \int_0^T x(t)\, e^{-j\omega_k t} dt \tag{10}$$

where $x(j\omega_k)$ and $x(t)$ are Fourier transform pairs, ω_k is the radian frequency for indices $k = 1, 2, \ldots, M$, and T is the data record length. Equation (10) can be evaluated in several ways. For post-flight analysis, the chirp z-transform is used, which provides arbitrary frequency resolution over a specified frequency bandwidth of interest.

The Fourier transform can also be applied in real time, as data are being collected during flight. When the sampling rate is much higher than the bandwidth of interest, the Euler formulation

$$x(j\omega_k) \simeq \Delta t \sum_{i=1}^{N} x(t_i)\, e^{-j\omega_k t_i} \tag{11}$$

accurately approximates Eq. (10), where Δt is the sampling period, t_i is the sample time for indices $i = 1, 2, \ldots, N$. The Euler form can be made recursive for real-time analysis during flight as

$$x_i(j\omega_k) = \lambda\, x_{i-1}(j\omega_k) + x(t_i)\, e^{-j\omega_k t_i} \tag{12}$$

to update after each data sample. The term λ is an exponential forgetting factor that can be adjusted between 0 and 1 to systematically discard past data and adapt more quickly to recent information, if desired.

Prior to applying the Fourier transform, low-frequency content in the data should first be removed to reduce spectral leakage from these components, which is due to the finite data record. As a result, the frequency-domain data represent perturbations from steady-state and low-frequency values. For post-flight analysis, analysis using simulation data showed the most accurate way of doing this was to fix both endpoints of the time series to zero, which removes boundary discontinuities and improves the convergence of the transform. Another technique is to remove a fitted linear trend from the data. For real-time analysis, detrending can be performed by applying a high-pass filter, such as a fourth-order Butterworth filter, with the break frequency set below the lowest frequency of interest.

B. Maximum Likelihood Equation-Error Method

Equation error is a maximum likelihood estimator for the case of negligible measurement noise and white Gaussian process noise. For the model considered, the observations reduce to

$$\mathbf{z} = \mathbf{y} + \mathbf{v} \tag{13a}$$

$$= \mathbf{X}\boldsymbol{\theta} + \mathbf{v} \tag{13b}$$

where $\mathbf{z}$ is the dependent variable to be modeled, $\mathbf{y}$ is the model output, $\mathbf{X}$ is a matrix of regressors or explanatory variables, $\boldsymbol{\theta}$ is a vector of model parameters to be estimated, and $\mathbf{v}$ are the equation errors. The dependent variables are the aerodynamic coefficients, which are computed from measured data as

$$C_Z = \frac{mg}{\bar{q}S} a_z \tag{14a}$$

$$C_m = \frac{I_{yy}}{\bar{q}S\bar{c}} \left[\dot{q} + \left(\frac{I_{xx} - I_{zz}}{I_{yy}} \right) pr + \frac{I_{xz}}{I_{yy}} \left(p^2 - r^2 \right) - M_T \right] \tag{14b}$$

and then detrended and transformed into the frequency domain. Equation (14) represents the full nonlinear aircraft motion, with or without turbulence, and accounts for the time variation in quantities such as mass or dynamic pressure. The estimation problem is decoupled between the two aerodynamic coefficients and Eq. (13) is processed twice: once for C_Z and once for C_m. Using C_Z, for example, the observation model is

$$\mathbf{z} = \begin{bmatrix} C_Z(j\omega_1) & C_Z(j\omega_2) & \ldots & C_Z(j\omega_M) \end{bmatrix}^T \tag{15a}$$

$$\mathbf{v} = \begin{bmatrix} v_Z(j\omega_1) & v_Z(j\omega_2) & \ldots & v_Z(j\omega_M) \end{bmatrix}^T \tag{15b}$$

$$\boldsymbol{\theta} = \begin{bmatrix} C_{Z_\alpha} & C_{Z_{\dot{\alpha}}} & C_{Z_q} & C_{Z_{\delta_e}} \end{bmatrix}^T \tag{15c}$$

$$\mathbf{X} = \begin{bmatrix} \mathbf{x}_1 & \mathbf{x}_2 & \mathbf{x}_3 & \mathbf{x}_4 \end{bmatrix} \tag{15d}$$

where the columns of $\mathbf{X}$ are formed as the Fourier transforms

$$x_1(j\omega_k) = \mathcal{F}\left[\Delta\alpha + \Delta\alpha_g\right] \tag{15e}$$

$$x_2(j\omega_k) = \mathcal{F}\left[\left(\dot{\alpha} + \dot{\alpha}_g\right) \frac{\bar{c}}{2V}\right] \tag{15f}$$

$$x_3(j\omega_k) = \mathcal{F}\left[\left(q - \dot{\alpha}_g\right) \frac{\bar{c}}{2V}\right] \tag{15g}$$

$$x_4(j\omega_k) = \mathcal{F}\left[\Delta\delta_e\right] \tag{15h}$$

A similar observation model is used for the pitching moment derivatives.

The equation-error solution minimizes the cost

$$J(\boldsymbol{\theta}) = \frac{1}{2} (\mathbf{z} - \mathbf{X}\boldsymbol{\theta})^\dagger (\mathbf{z} - \mathbf{X}\boldsymbol{\theta}) \tag{16}$$

which is a quadratic function of the model residual. This is an ordinary least-squares problem with the optimal solution for the model parameters

$$\hat{\boldsymbol{\theta}} = \left[\Re\left(\mathbf{X}^\dagger\mathbf{X}\right)\right]^{-1} \Re\left(\mathbf{X}^\dagger\mathbf{z}\right) \tag{17}$$

The estimated parameter covariance matrix is

$$\mathrm{cov}(\hat{\boldsymbol{\theta}}) = \sigma^2 \left[\Re\left(\mathbf{X}^\dagger\mathbf{X}\right)\right]^{-1} \tag{18}$$

where σ^2 is the equation-error variance, which can be estimated from the model residuals as

$$\hat{\sigma}^2 = \frac{(\mathbf{z} - \mathbf{X}\boldsymbol{\theta})^\dagger (\mathbf{z} - \mathbf{X}\boldsymbol{\theta})}{M - n_p} \tag{19}$$

for a model containing n_p parameters.

The equation-error method using frequency-domain data was selected for several reasons. First, equation error is a relatively simple analysis with an analytical solution that does not require iteration. Furthermore, there are many useful statistical metrics and tools for determining the model structure, i.e. which model terms should be included in Eq. (4).

The analysis was performed in the frequency domain because fewer parameters are needed, making the analysis more efficient. Because only the bandwidth of interest is used in the Fourier transform, high-frequency noise is automatically rejected and statistically accurate uncertainties for the model parameters are obtained. Additionally, the estimation could be performed in real time during flight if the recursive Fourier transform is used and the least-squares solution is sequentially computed.

An attempt was made to also use output error for the parameter estimation. However, several challenges were encountered. Performing the analysis using time-domain data required 7 additional state and output equation bias parameters to keep the model outputs from diverging, which increased the size and complexity of the estimation problem. Also, significant excursions (10% in airspeed, 20% in dynamic pressure) from the reference condition, due to the turbulence, violated the assumed linear time-invariant model structure of Eqs. (6) and (9) and degraded estimation results using output error in the time and frequency domains. A nonlinear formulation of the model accounting for the time-dependent variation in airspeed and dynamic pressure could have been formulated for the time-doimain output-error analysis, at the expense of additional computation time and model complexity. However, the output-error results also exhibited lower sensitivities for the damping derivatives, such as C_{m_q}, which results in less accurate estimates. Therefore, the output-error approach was not used in this work and only the equation-error results using Fourier-transform data are presented.

VI. Turbulence Reconstruction

A classical technique for reconstructing turbulence was explored in Ref. [12] and formalized in Refs. [13, 14]. The fundamental concept is to remove the motion of the airplane from measured airdata to recover the motion of the atmosphere, which is the turbulence. As shown in Ref. [13], the linearized vane output in longitudinal flight from Eq. (9) can be rearranged as

$$\alpha_g = \alpha_v - \alpha + \frac{x_\alpha}{V} q \tag{20}$$

By measuring α_v and q with an air flow-angle vane and a rate gyroscope, and by computing α from airspeed and integrated vertical accelerometer measurements, α_g can be reconstructed. However, this process applies many simplifying assumptions that reduce the reconstruction accuracy. As a result, Ref. [13] recommends flying with fixed controls to minimize the motion of the airplane to be removed. However, this guideline is detrimental for a successful system identification experiment, which requires informative data generated from moving the control effectors.

The classical technique can be improved in several ways. One way is to retain the neglected terms in the vane measurement equation. Assuming rigid-body dynamics and negligible forward gusts compared to the airspeed, the vane output is

$$\alpha_v = \arctan\left(\frac{w - x_\alpha q + y_\alpha p - w_g}{u - y_\alpha r + z_\alpha q}\right) \tag{21}$$

where y_α and z_α are the remaining body-fixed locations of the vane relative to the mass center. Rearranging this equation, the vertical turbulence can be solved for as

$$w_g = w - x_\alpha q + y_\alpha p - \tan\alpha_v\,(u - y_\alpha r + z_\alpha q) \tag{22}$$

After substituting Eq. (22) into (1), the angle of attack gust is

$$\alpha_g = -\frac{1}{u}\left[w - x_\alpha q + y_\alpha p - \tan\alpha_v\,(u - y_\alpha r + z_\alpha q)\right] \tag{23}$$

This expression retains the trigonometric nonlinearity in the vane measurement, as well as contributions from angular rates. Turbulence can excite all axes of the aircraft motion, making the angular rate contributions significant, particularly for smaller aircraft with lower mass and inertia [15]. For the flight data from the subscale aircraft discussed later, about 30% of the variation in the reconstructed turbulence from the individual airdata vanes was attributed to the angular rate terms. For aircraft with redundant vanes on the wing tips, these terms can be minimized by first averaging data from each wingtip vane, rather than computing the turbulence from each individual wing-tip vane. For aircraft with nose booms, the pitch rate contributions may be significant.

A second way to improve the classical technique involves computing α from inertial measurements. Instead of integrating vertical accelerometer data, as in Ref. [13], the nonlinear aircraft kinematic equations [3, 16]

$$\dot{u} = rv - qw + ga_x - g\sin\theta \tag{24a}$$

$$\dot{v} = pw - ru + ga_y + g\sin\phi\cos\theta \tag{24b}$$

$$\dot{w} = qu - pv + ga_z + g\cos\phi\cos\theta \tag{24c}$$

can be solved using measured data. These equations account for gravity and the velocity couplings of the aircraft, in addition to the specific forces measured by the accelerometers. The initial conditions can be taken as

$$u(0) = V(0)\cos\alpha(0)\cos\beta(0) \tag{25a}$$

$$v(0) = V(0)\sin\beta(0) \tag{25b}$$

$$w(0) = V(0)\sin\alpha(0)\cos\beta(0) \tag{25c}$$

A third way to improve the classical technique is to transform the reconstructed turbulence into the frequency domain. Measurement noise and sensor bias errors create offsets and drifts in reconstructions of u, v, and w, and therefore also in the reconstructed turbulence. By transforming the reconstruction into the frequency domain, these low-frequency errors are removed [16]. Attempts to mitigate these errors by applying a data compatibility analysis were unsuccessful because the measurements included the turbulence although the model for that information assumed calm air. Note that in transforming the data into the frequency domain, the Fourier transform should be applied over a limited bandwidth in which the turbulence has appreciable content and which respects the rigid-body assumption used in Eq. (21). Reconstruction at higher frequencies may require incorporating other additional dynamics, such as digital filters or structural modes. Using a frequency-domain analysis, time delays can also be estimated [17], for example when a vane is installed ahead of the aircraft nose and far from the mass center.

These discussed enhancements improve the accuracy of the reconstructed turbulence. This process changes turbulence from an unknown input to a known input, which enables accurate system identification. The analysis can also be applied to reconstruct forward and lateral gusts in a similar manner to Eqs. (21)–(23). Note that the rotational gusts cannot be directly reconstructed in this way because gyroscopes measure inertial information rather than air-relative information. Because the reconstruction depends on measured data, the primary cost for accurate turbulence reconstruction is high-quality and low-noise instrumentation.

VII. Test Aircraft and Simulation Model

System identification using reconstructed turbulence measurements was investigated using simulated data and measured flight test data for the T-2 airplane, which is shown in Fig. 1. The T-2 is a 5.5% dynamically-scaled version of a generic, transport-type aircraft, with twin jet engines mounted under the wings and retractable tricycle landing gear. Aircraft geometry and nominal mass properties are listed in Table 1. The nominal flight condition considered was straight and level flight at about 5 deg angle of attack, 135 ft/s airspeed, and 1500 ft altitude.

Fig. 1 T-2 airplane (credit: NASA Langley Research Center).

The aircraft is instrumented with research-quality hardware, and was flown remotely from the Airborne Subscale Transport Aircraft Research (AirSTAR) flight-test facility. The instrumentation includes a micro inertial navigation system, an additional inertial measurement unit, and air data probes attached to booms mounted on each wingtip. Flight

Table 1 T-2 aircraft geometry and nominal mass properties.

Symbol	Value	Unit
$\bar{c}$	0.915	ft
b	6.849	ft
S	5.902	ft^2
m	1.585	slug
I_{xx}	1.179	slug-ft^2
I_{yy}	4.520	slug-ft^2
I_{zz}	5.527	slug-ft^2
I_{xz}	0.211	slug-ft^2

data were measured at 200 Hz, downsampled to 50 Hz, and digitally low-pass filtered to 16 Hz for analysis of the rigid-body dynamics.

Flight test data for 23 maneuvers in various levels of turbulence from flights 15, 30, and 33 were analyzed. Example simulation and flight test data for one maneuver in severe turbulence are shown in Fig. 2. The elevator input was an orthogonal phase-optimized multisine [3], which contained power between 0.3–2.1 Hz. The flight data also included multisine inputs on the aileron and rudder, but only longitudinal motion is examined here. In comparison, pilot inputs were low in amplitude and frequency. Other input types, such as 3211 multisteps, were investigated using simulation data; similar trends but less accurate results were observed.

The turbulence level was quantified using the empirical metric $\sigma_{w\,[2\text{–}7\text{ Hz}]}$, which was introduced in Ref. [2] as a measurement of spectral power in the body-axis vertical velocity between 2–7 Hz. The vertical component of velocity was used because the turbulence was most apparent in the vertical axis and was speculated to be the result of convection from diurnal heating. The range 2–7 Hz was selected because this range was higher in frequency than the rigid-body dynamics but still contained appreciable content due to the turbulence. The metric correlated well with turbulence ratings from the pilot, who was flying the airplane from the ground using a heads-up display drawn from telemetered data and a map of the local terrain. Reference [2] describes how to compute this metric in real time from airspeed and angle of attack measurements using spectral density estimation and frequency binning. A different approach was employed here, where the detrended data were projected on a Fourier sine series [3] and coefficients outside the 2–7 Hz bandwidth were discarded. The turbulence metric was computed as the standard deviation of the reconstructed signal. Applied to simulation data, this technique produced turbulence metrics with less scatter than using the spectral density approach. One advantage of using this metric to quantify turbulence is that it is based on measured flight test data and does not impose a model on the turbulence. Possible drawbacks are that the metric is based on the motion of the aircraft, and is therefore aircraft and configuration dependent.

A simulation of the T-2 airplane short period dynamics using Eqs. (6) and (9) was also employed in this investigation to compliment analyses of the flight test data. Parameter values listed in the middle column of Table 2 were used, which were obtained from the flight test results described later in Section V. First-order actuator dynamics, having a 0.10 s time delay and a pole at 5 Hz, were included for the elevator. Realistic measurement noise and random sensor biases were added to the measured outputs. Fourth-order Butterworth low-pass filters with break frequencies at 16 Hz were applied to all simulated measurements to replicate the flight test data.

Random turbulence sequences were simulated using Fourier series expansions as in Ref. [18]. Realizations of the angle of attack gust were generated as

$$\Delta\alpha_g(t) = -\sum_{k=1}^{N/2} \frac{c_k}{V} \sin\left(\frac{2\pi k}{T} t + \phi_k\right) \tag{26}$$

and the angle of attack gust rate as

$$\dot{\alpha}_g(t) = -\sum_{k=1}^{N/2} \frac{2\pi k c_k}{VT} \cos\left(\frac{2\pi k}{T} t + \phi_k\right) \tag{27}$$

Using Eq. (27) to obtain $\dot{\alpha}_g$ avoided numerical differentiation or augmenting the model state vector. The phase spectrum

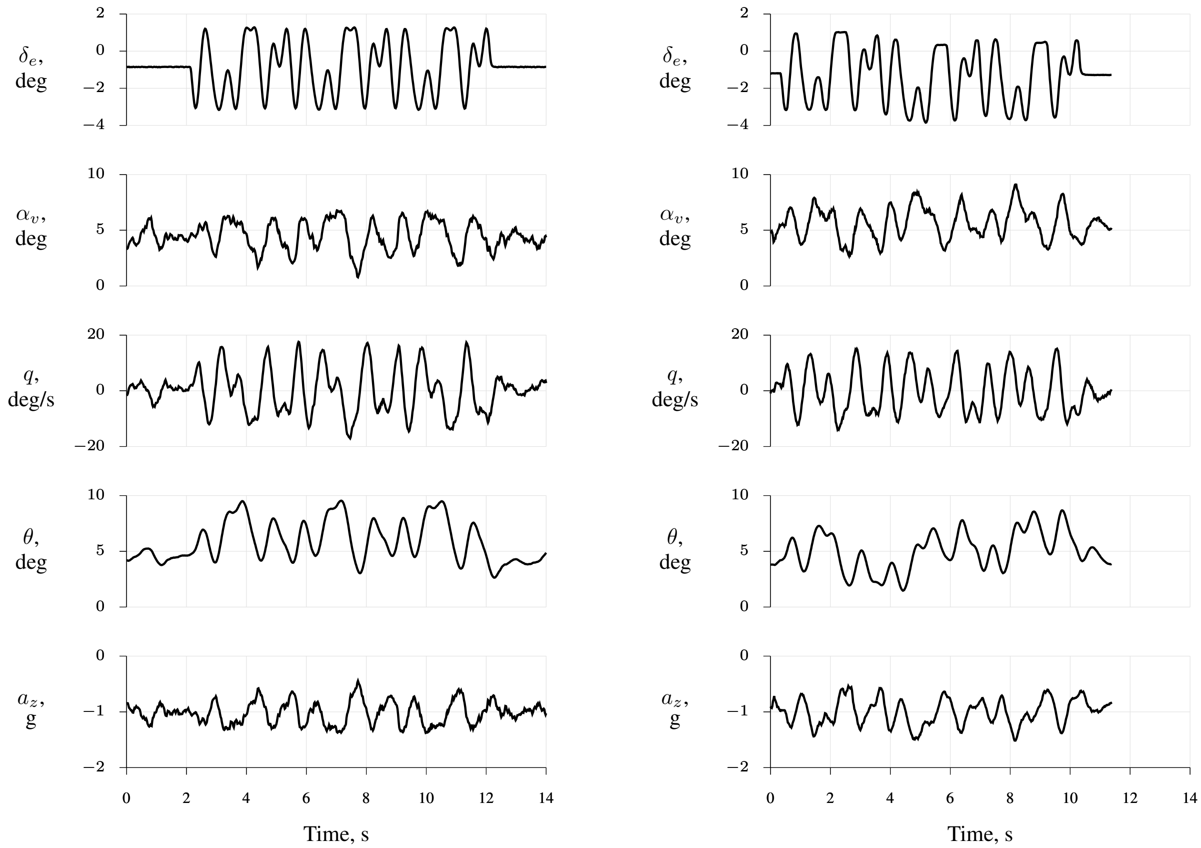

(a) Simulation data. (b) Flight data.

Fig. 2 Example simulation and flight test data in severe turbulence.

ϕ_k was randomly drawn over the interval $[0, 2\pi)$ rad. The amplitude spectrum was

$$c_k = \sqrt{2\Delta\omega\, \Phi_{ww}(j\omega_k)} \tag{28}$$

where $\Delta\omega = 2\pi/T$ is the angular frequency resolution of the Fourier series, and where

$$\Phi_{ww}(j\omega_k) = \frac{2\sigma_w^2 L_w}{\pi V} \frac{1 + \frac{8}{3}\,(2.678\, L_w\omega_k/V)^2}{\left[1 + (2.678\, L_w\omega_k/V)^2\right]^{11/6}} \tag{29}$$

is the von Kármán vertical gust spectrum [19]. At 1500 ft altitude, $L_w = 875$ ft is the turbulence scale length. Because the T-2 is a subscale aircraft with smaller mass and inertia, turbulence intensities σ_w prescribed in Ref. [19] were too large and did not match pilot turbulence ratings [20]. Instead, the cubic calibration shown in Fig. 3 was determined to correlate the simulation and flight test data in terms of σ_w, $\sigma_{w_{[2\text{–}7\text{ Hz}]}}$, and pilot turbulence ratings. The simulation results included 500 runs with σ_w uniformly sampled over 0–6 ft/s. Turbulence levels for the 23 flight test maneuvers are also shown, which spanned from light turbulence through severe turbulence. The calibration was approximately linear, except for light turbulence, and did not pass through the origin because $\sigma_{w_{[2\text{–}7\text{ Hz}]}}$ had power from turbulence responses and measurement noise. As shown in Fig. 2, the simulation data were representative of the flight test data in similar turbulence levels.

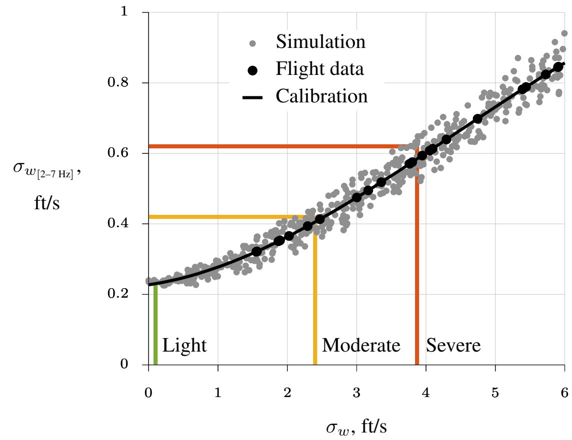

Fig. 3 Calibration of turbulence intensity, turbulence metric, and pilot turbulence rating for the T-2 airplane.

VIII. Results

A. Turbulence Reconstruction

Example turbulence reconstructions are shown in Fig. 4 for simulation data and flight test data in severe turbulence. The top plots show the reconstructed time series. The simulation data in Fig. 4(a) shows the reconstruction is very similar to the applied gust, except for the expected bias and drift. These errors were removed during the Fourier transform, which is shown in the bottom two plots in terms of magnitude and phase components, up to the 3 Hz bandwidth used for parameter estimation in Section VIII.C. For the simulation data, the reconstructed turbulence is a very close match over this range of frequency. The reconstruction for the flight test data in Fig. 4(b) is similar in appearance to the simulation data. As expected, the turbulence contains the most power at low frequencies and then rolls off with increasing frequency.

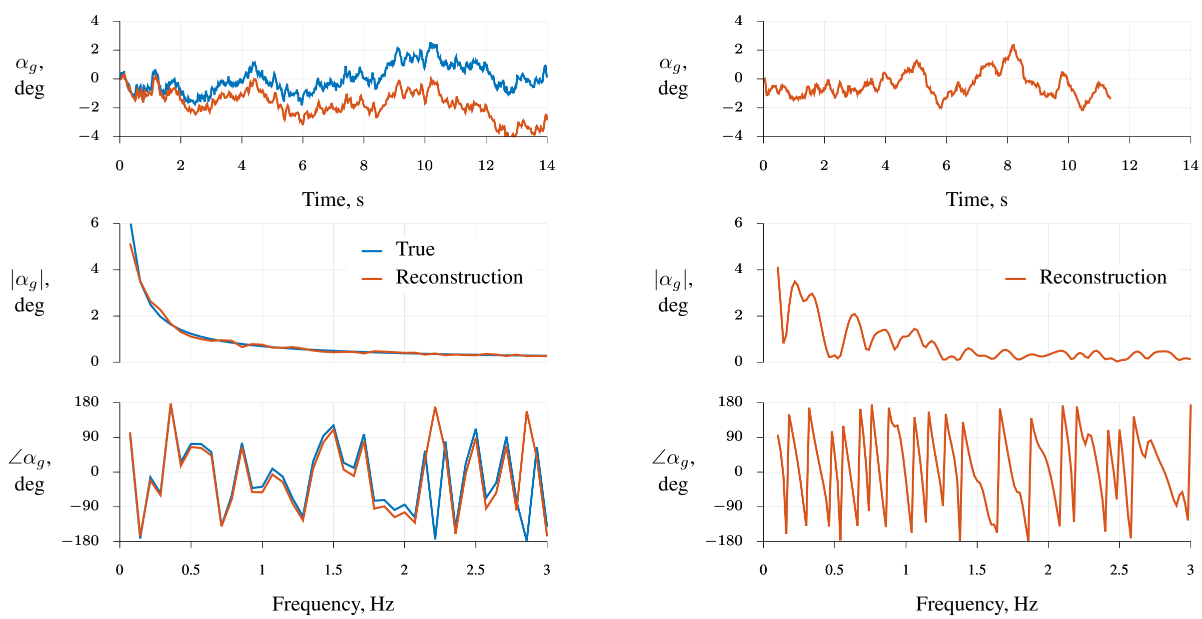

(a) Simulation data.

(b) Flight data.

Fig. 4 Reconstructed angle of attack gusts in severe turbulence.

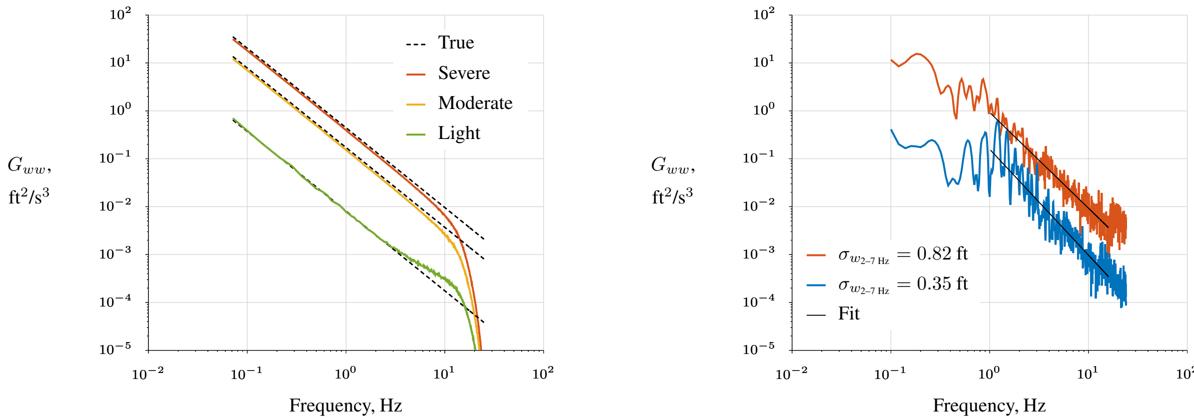

(a) Simulation data.

(b) Flight data.

Fig. 5 Power spectra of reconstructed vertical gusts in various levels of turbulence.

The power spectra of reconstructed vertical gusts are shown for simulation data and flight test data in various levels of turbulence in Fig. 5. The spectra were computed using the one-sided periodogram [21]

$$G_{ww}(j\omega) = \frac{2}{T}|w_g(j\omega)|^2 \tag{30}$$

for each simulation run or flight test maneuver, and then averaged at each frequency over the ensemble of runs. This computation was possible because the chirp z-transform used to transform the data allows for arbitrary specification of the analysis frequencies. Unlike in Fig. 4, these results are shown up to the 25 Hz Nyquist frequency. Each curve in Fig. 5(a) corresponds to a different level of turbulence and included an ensemble of 500 simulation runs. The corresponding von Kármán spectra used to generate the turbulence are also shown. In Fig. 5(b), the curves correspond to light-to-moderate and severe turbulence, and each included ensembles of six maneuvers having roughly the same turbulence level.

For the simulation data, the reconstructed turbulence spectra closely matched the true spectra for moderate and severe turbulence up to about 10 Hz, where distortions from the 16 Hz low-pass filters corrupted the estimates. For light turbulence, the spectra were matched well up to about 4 Hz, above which turbulence and measurement noise were indistinguishable. Spectral estimates of the flight data contained more scatter than the simulation data because only six maneuvers were averaged and because each maneuver had slightly different levels of turbulence. However, the flight test results have a similar appearance to the simulation results. Trend lines fitted to estimated spectra from each individual maneuver over the bandwidth 1–16 Hz had an average slope -1.86 ± 0.26. This was in statistical agreement with the theoretical value of $-5/3$ or about -1.67 used in the von Kármán turbulence model.

B. Collinearity Analysis

When regressor data are nearly collinear or linearly dependent, an estimator cannot decipher between the effects, and resulting parameter estimates are biased with large uncertainties [3]. Pairwise correlation between two explanatory variables, x_j and x_k, is measured by the correlation coefficient

$$r_{jk} = \frac{\sum_{i=1}^{N} \left[x_j(i) - \bar{x}_j\right]\left[x_k(i) - \bar{x}_k\right]}{\sqrt{\sum_{i=1}^{N} \left[x_j(i) - \bar{x}_j(i)\right]^2 \sum_{i=1}^{N} \left[x_k(i) - \bar{x}_k(i)\right]^2}} \tag{31}$$

which ranges between -1 and $+1$. For flight dynamics analysis, correlations larger than 0.9 in absolute value are considered highly correlated.

Visually, pairwise correlation coefficients with high absolute value result when regressor time histories, plotted against each other, resemble a straight line. Example plot matrices are shown in Fig. 6 for simulation data in calm air and in severe turbulence. The matrix diagonal contains the regressor parameters, the lower triangle shows the pairwise correlation coefficients, and the upper triangle shows time-domain regressor data plotted against each other. Flight test data followed similar trends as the turbulence level was changed. In calm air, all the regressors had sufficiently low correlations except for $C_{a_{\dot{\alpha}}}$ and C_{a_q}, which had a correlation coefficient of 0.93 and resembled a straight line, as expected for a small-perturbation maneuver at low nominal angles of attack [22]. In severe turbulence, all of the parameter correlations decreased in absolute value, meaning that their effects were more distinguishable. One significant change was that the correlation between $C_{a_{\dot{\alpha}}}$ and C_{a_q} not only decreased in value but also switched sign.

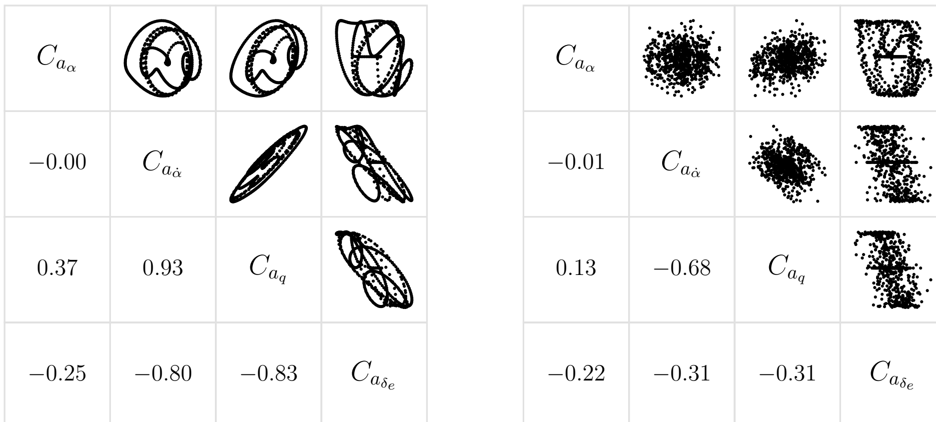

(a) Calm air.

(b) Severe turbulence.

Fig. 6 Plot matrix of regressor pairwise correlations using simulation data.

To investigate further, pairwise correlations were examined for various turbulence levels. It was found that much of the decorrelation exhibited in Fig. 6(b) was due to high-frequency phase differences in the turbulence reconstruction, which were expected to be less accurate as discussed above in Section VIII.A. When the explanatory variable data were restricted to the modeling bandwidth of 0–3 Hz, either by smoothing the data or transforming it into the frequency domain, the same trends were present but were less abrupt. These results are shown in Fig. 7 for each combination of explanatory variables, as a function of the turbulence level. The simulation and flight test data followed similar trends, where as the turbulence level increased, regressor pairwise correlations decreased, including between $C_{a_{\dot{\alpha}}}$ and C_{a_q}.

In addition to pairwise collinearity, multicollinearity was also examined, which is when one regressor resembles a linear combination of other regressors. Multicollinearity problems cannot always be detected using pairwise correlations and require other tests. Typical multicollinearity detection techniques [3] were applied and no multicollinearity was found.

C. Parameter Estimation

The proposed model structure was assessed using stepwise regression and orthogonal multivariate functions in the frequency domain [3] for the combined flight test maneuvers. The estimation was performed over the 0–3 Hz bandwidth where the modeling data had appreciable content. It was found that C_{Z_α} accounted for over 99% of the C_Z data variation using the coefficient of determination R^2, and that C_{m_α}, C_{m_q}, and C_{m_δ} accounted for over 96% of the C_m data variation. Based on this assessment, the additional model terms were not statistically relevant to the model.

However, to assess the identifiability of stability and control derivatives using the full model structure in Eq. (4), simulations were performed with 500 runs over various levels of turbulence. Figure 8 shows true values and estimates with 2σ error bounds. For turbulence metrics less than 0.5 ft/s, there was larger scatter in the estimates, particularly in $C_{a_{\dot{\alpha}}}$ and C_{a_q}, due to the collinearity problems discussed in Section VIII.B. For higher turbulence levels, biases in the C_Z derivatives were small. Many estimates of $C_{a_{\dot{\alpha}}}$ were statistically zero, which confirmed these parameters could have been removed from the model. At higher turbulence levels, C_{m_α} and $C_{m_{\delta_e}}$ contained noticeable biases. It was found that when the true turbulence was used, rather than the reconstruction, biases were zero in the C_Z derivatives and were reduced in the C_m derivatives. The remaining offsets in the C_m derivatives were due to errors introduced from numerically differentiating gyroscope data to compute C_m.

Results of applying the parameter estimation to the flight data are shown in Fig. 9. The scatter due to data collinearity

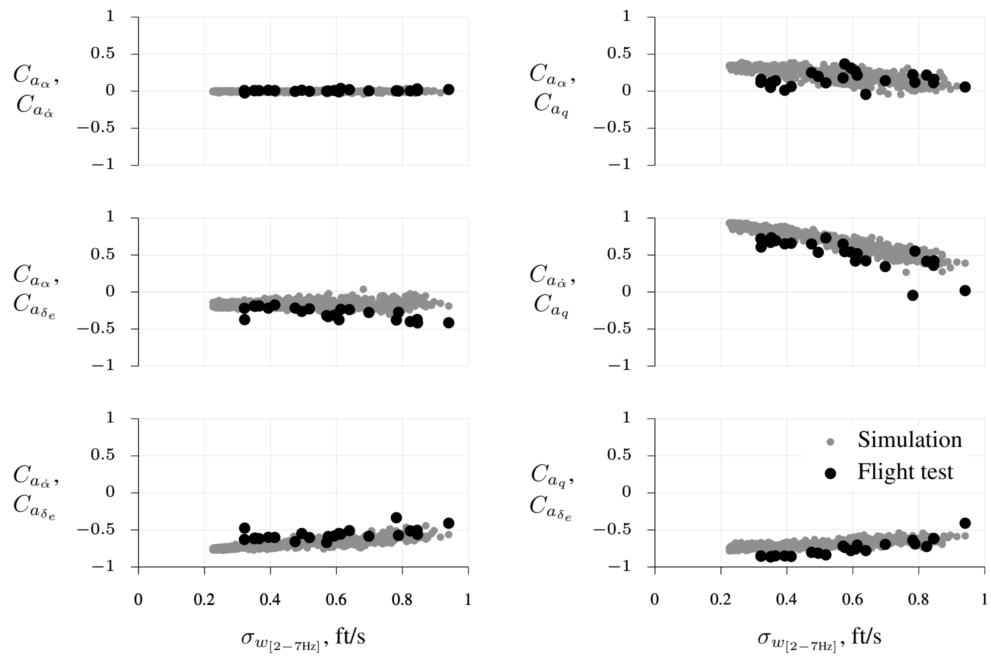

Fig. 7 Regressor pairwise correlation coefficients over 0–3 Hz and various turbulence levels.

problems appeared to decrease for turbulence metrics around 0.5 ft/s or higher, similar to the simulation data. For turbulence metrics above 0.5 ft/s, scatter and uncertainties are small and consistent, and similar to or better than the simulation results. Some of the variation in the estimates could be attributed to differences in flight conditions or how some maneuvers included larger angles of attack. Estimation results using 15 combined maneuvers that had turbulence metrics over 0.5 ft/s are given with standard errors in Table 2. These parameters are in rough agreement with previous results [2, 22], and differences can be attributed to the changes in model structures. Estimates of the derivative $C_{m_{\dot\alpha}}$, which are difficult to accurately obtain, were in statistical agreement with previous results [22].

To investigate a simpler aerodynamic model structure, the rotational gust contribution $-\dot\alpha_g$ was neglected. Model fits did not degrade, but the $C_{a_{\dot\alpha}}$ parameters became statistically insignificant and were also removed, resulting in the reduced model

$$\Delta C_a = C_{a_\alpha}\left(\Delta\alpha + \Delta\alpha_g\right) + C_{a_q}\frac{q\bar{c}}{2V_0} + C_{a_{\delta_e}}\Delta\delta_e \tag{32}$$

which is a conventional model for identification but is here applied to data in turbulence. This is effectively the same model structure applied in Ref. [2], except C_{Z_q} is retained. Equation (32) includes the effect of turbulence on the effective angle of attack, neglects the angular gust contribution, and lumps together the $C_{a_{\dot\alpha}}$ and C_{a_q} derivatives. Note that the first regressor is approximately the vane measurement when all the nonlinearities and angular rate terms are removed. Because the rotational gust was neglected, turbulence reconstruction here was unnecessary. Parameter estimates for the reduced model and the flight test maneuvers are shown in Fig. 10. The same trends as seen in Fig. 9 are present, although the estimates have lower uncertainties and less scatter. In comparison with Fig. 9, all parameters are offset slightly.

Figure 11 shows model fits to flight test data using the 14 maneuvers with turbulence metrics larger than 0.5 ft/s. This was done using both the full model in Eq. (4) and the conventional model in Eq. (32). The two fits to C_Z are practically identical, each having $R^2 = 0.99$. The C_m data was fit slightly better by the conventional model than the full model, with coefficients of determination R^2 values of 0.98 and 0.94, respectively. Parameter estimates for these two models are given in Table 2 with standard errors. The C_{a_α} and $C_{a_{\delta_e}}$ derivatives were similar for both models and were in statistical agreement with each other. Similarly, the C_{a_q} derivatives were similar and in statistical agreement after $C_{a_{\dot\alpha}}$ and C_{a_q} had been lumped together in the full model. These estimates are in agreement with those obtained in previous analyses [2, 22].

A prediction maneuver using these two identified models is shown in Fig. 12. The flight condition was 4.5 deg

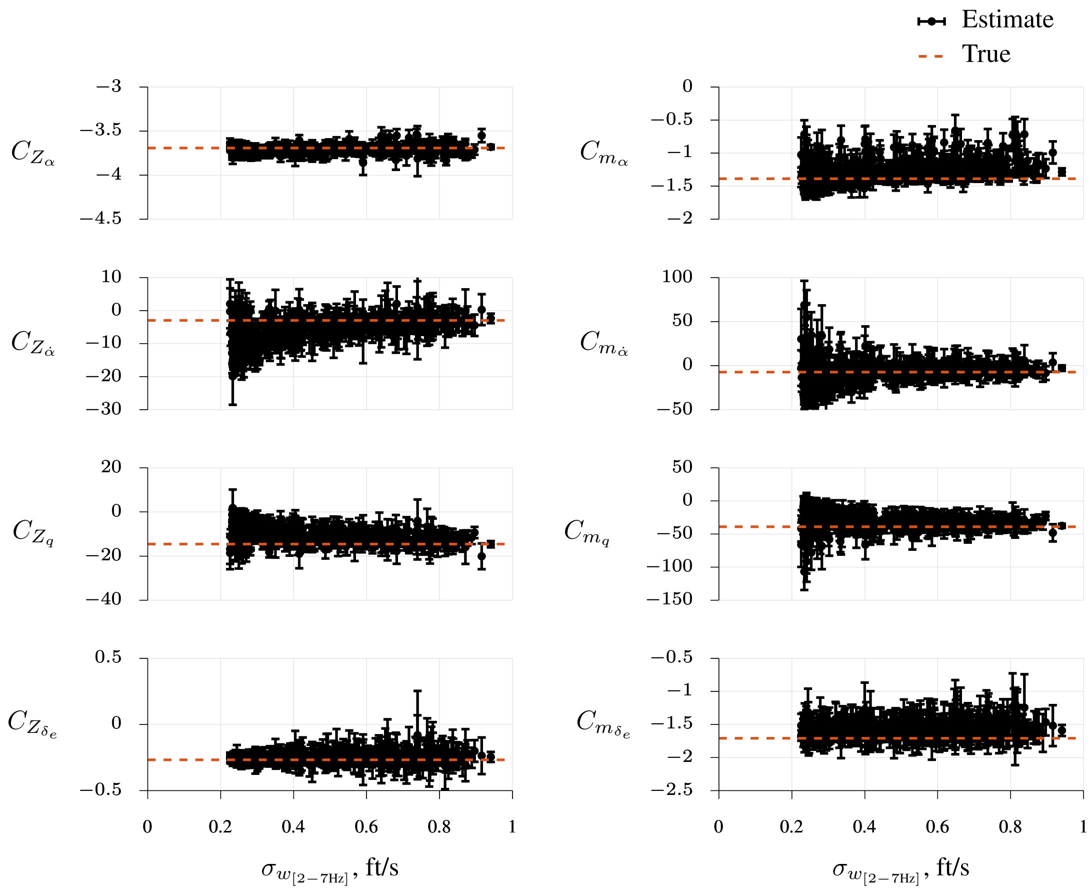

Fig. 8 Parameter estimates and 2σ errors using simulation data.

Table 2 Stability and control derivatives identified from T-2 flight test data with $\sigma_{\mathrm{w}\,[2\text{–}7\,\mathrm{Hz}]} > 0.5$ ft/s.

Parameter θ	Full model $\hat\theta \pm s(\hat\theta)$	Reduced model $\hat\theta \pm s(\hat\theta)$
C_{Z_α}	-3.69 ± 0.02	-3.67 ± 0.02
$C_{Z_{\dot\alpha}}$	-2.96 ± 0.89	—
C_{Z_q}	-14.6 ± 1.99	-21.6 ± 1.53
$C_{Z_{\delta_e}}$	-0.27 ± 0.03	-0.36 ± 0.03
C_{m_α}	-1.39 ± 0.03	-1.34 ± 0.02
$C_{m_{\dot\alpha}}$	-7.32 ± 1.41	—
C_{m_q}	-39.1 ± 3.20	-53.3 ± 1.95
$C_{m_{\delta_e}}$	-1.71 ± 0.06	-1.88 ± 0.04

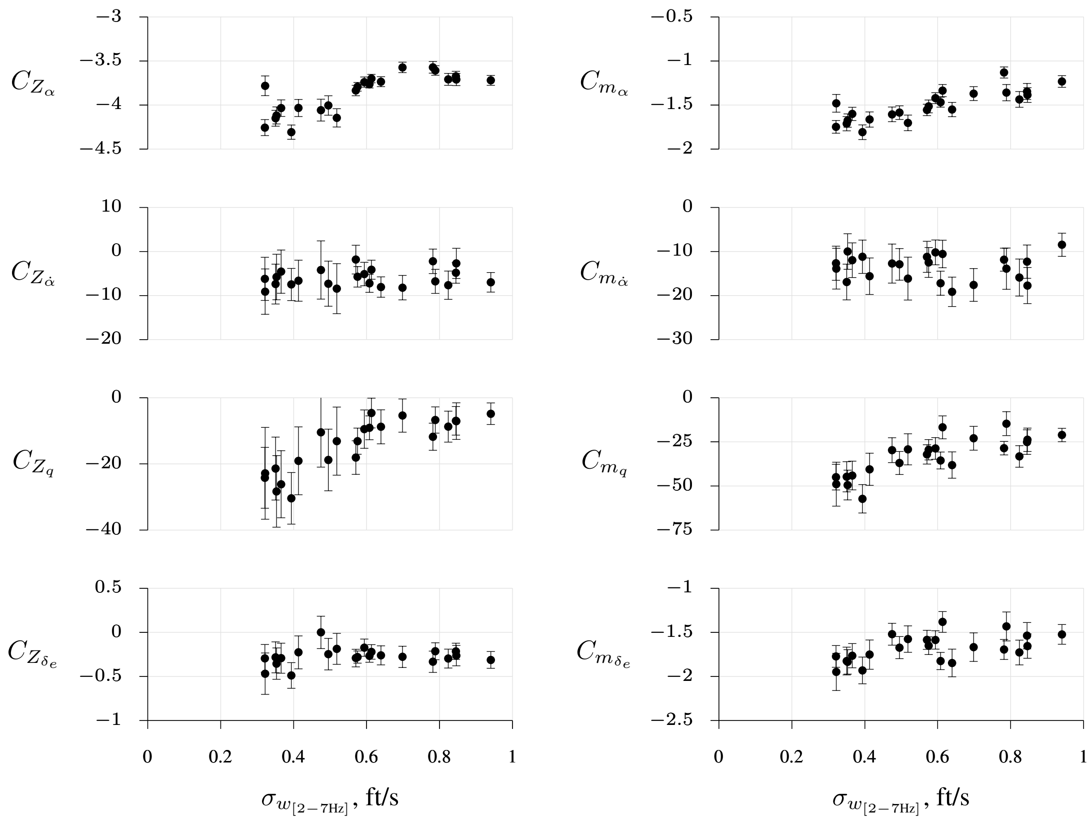

Fig. 9 Parameter estimates and 2σ errors using flight test data.

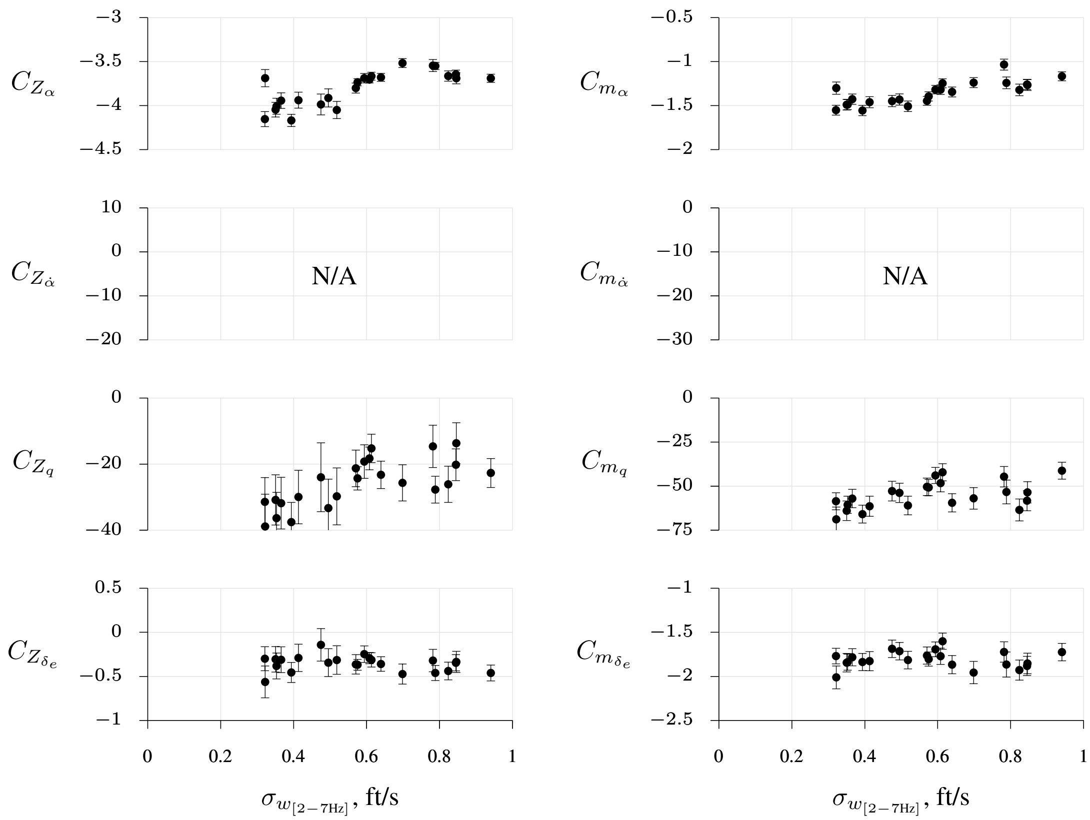

Fig. 10 Parameter estimates and 2σ errors using flight test data and a reduced aerodynamic model.

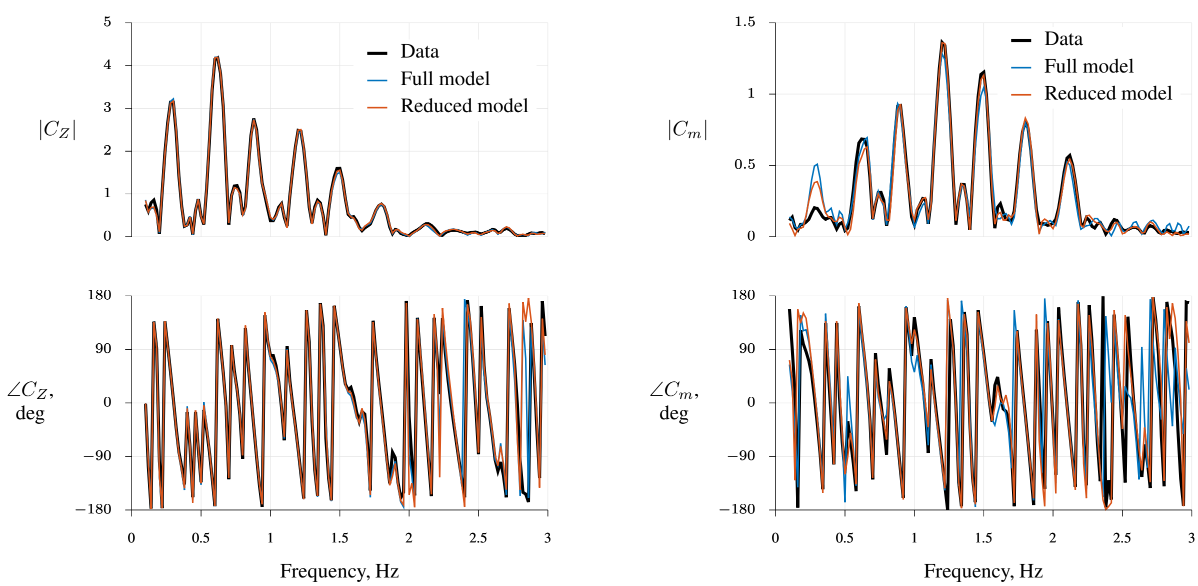

(a) Vertical force coefficient.

(b) Pitching moment coefficient.

Fig. 11 Equation-error fits to data using 14 flight test maneuvers having $\sigma_{\mathrm{w}\,[2\text{–}7\,\mathrm{Hz}]} > 0.5$ ft/s.

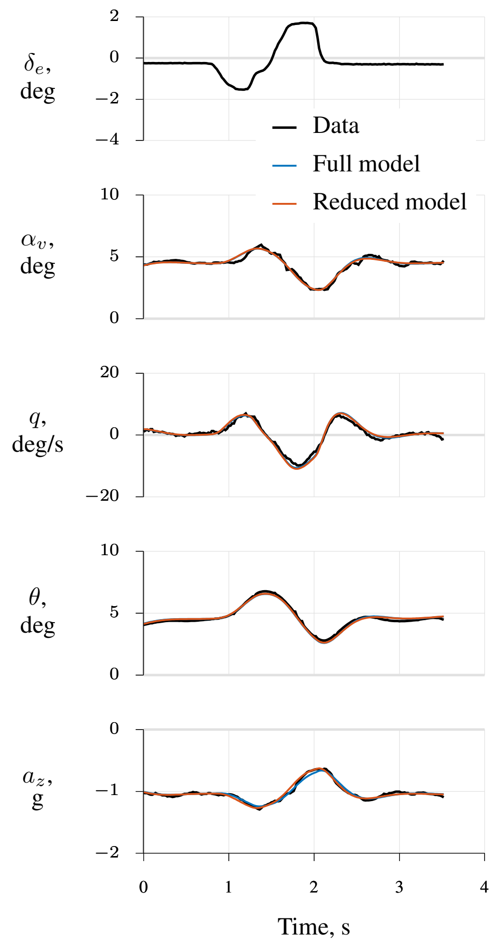

Fig. 12 Prediction case in light turbulence.

angle of attack, 140 ft/s airspeed, and 1250 ft altitude, which was similar to the maneuvers used for identification. The turbulence for this maneuver was light, with a turbulence metric of 0.28 ft. The maneuver included a small elevator doublet exciting the short period response. The identified model parameters in Table 2 were substituted into the the state-space model in Eqs. (6) and (9) and simulated using the measured elevator time history. Matches to the measured data were excellent and had R^2 values above 0.95 for all time histories. The modal characteristics of the two models at this condition were similar: the full model had short period damping 0.47 and natural frequency 6.5 rad/s (1.0 Hz), whereas the reduced model had damping ratio 0.51 and natural frequency 6.6 rad/s (1.0 Hz). This prediction case demonstrates that the short period models, identified from data with turbulence metrics larger than 0.5 ft, predict the aircraft motion well in lower amounts of turbulence.

IX. Conclusions

System identification of aircraft aerodynamic models using reconstructed turbulence measurements was investigated and discussed. A classical technique for turbulence reconstruction, based on airdata and inertial sensor measurements, was enhanced and applied for maneuvering flight. Nondimensional stability and control derivatives were estimated using the reconstructed turbulence and the maximum likelihood equation-error method in the frequency domain. The analysis was performed using simulation and flight test data for the NASA T-2 subscale airplane. The main findings of this research can be summarized as:

1) The angle of attack gust was accurately reconstructed over 0–3 Hz for modeling short period dynamics.
2) For turbulence metrics above 0.5 ft/s, angle of attack rate derivatives and pitch rate derivatives (e.g., $C_{m_{\dot{\alpha}}}$ and C_{m_q}) decorrelated and were accurately identified from small-perturbation maneuvers at low angles of attack using an optimized multisine excitation for the elevator input.
3) Stability and control derivatives for a short period model were accurately identified using equation error with Fourier transform data for flight with turbulence levels above 0.5 ft/s.
4) A simpler, conventional aerodynamic model which did not use reconstructed turbulence measurements and combined the acceleration and rate derivatives was also confirmed to provide accurate estimates of parameters for that model, which were statistically consistent with the parameters obtained from the full aerodynamic model.

The primary advantage of the proposed approach is the simplicity in the analyses, both in the reconstruction of the turbulence and the parameter estimation. These methods are computationally simple but incorporate the coupled, nonlinear dynamics of the aircraft, and provide a degree of robustness against sources of error, such as measurement noise or sensor biases. In part due to this simplicity, the turbulence reconstruction and parameter estimation can be run in real time, as data are collected during flight. Furthermore, these techniques alleviate the need to apply more complex algorithms for parameter estimation, such as nonlinear state estimators or the maximum likelihood filter-error method. The cost of this approach is high-quality instrumentation so that the turbulence can be accurately reconstructed and distinguished from other responses present in the measured data and measurement noise. Additionally, more data would be needed to accurately estimate the full set of applicable stability and control derivatives, but this is possible in sufficiently high levels of turbulence. A simplified, conventional aerodynamic model could also be used instead. The method produces poor reconstructions of turbulence when the turbulence level is low because the turbulence is indistinguishable from the noise. At these low turbulence levels, correlation problems can lead to poor estimation results when using the full model, and the simpler conventional aerodynamic model should be used.

The proposed methods can be used for several applications. Turbulence can be computed in real time to expand flight testing opportunities with relaxed restrictions on turbulence levels. Although only vertical gusts and short-period dynamics were investigated in this paper, the approach could be extended to the other gust components and dynamics of the aircraft. The reconstructed turbulence measurements could also be used as inputs for a turbulence-suppression flight control system, or to develop custom models of turbulence for simulation purposes such as handling qualities analysis or training for flight in hazardous conditions associated with turbulence. Real-time turbulence measurements could be used to quantify the level of turbulence during a flight test, independent of the aircraft dynamics or a turbulence model, which would be useful in cooperative flights with multiple aircraft.

Acknowledgments

This research was supported by the NASA Advanced Air Transport Technology (AATT) Project. The T-2 flight data used was generated by the NASA Langley (LaRC) AirSTAR team under the NASA Aviation Safety Program, Vehicle Systems Safety Technologies (VSST) project.

References

[1] Maine, R., and Iliff, K., "Formulation and Implementation of a Practical Algorithm for Parameter Estimation with Process and Measurement Noise," *SIAM Journal on Applied Mathematics*, Vol. 41, No. 3, 1981, pp. 558–579. doi:10.1137/0141045.

[2] Morelli, E., and Cunningham, K., "Aircraft Dynamic Modeling in Turbulence," *Atmospheric Flight Mechanics Conference*, AIAA Paper 2012-4650, Aug. 2012. doi:10.2514/6.2012-4650.

[3] Morelli, E., and Klein, V., *Aircraft System Identification: Theory and Practice*, 2$^{\text{nd}}$ ed., Sunflyte Enterprises, Williamsburg, VA, 2016.

[4] Bach, R., "State Estimation Applications in Aircraft Flight-Data Analysis: A User's Manual for SMACK," NASA RP-1252, Mar. 1991.

[5] Martos, B., and Morelli, E., "Using Indirect Turbulence Measurements for Real-Time Parameter Estimation in Turbulent Air," *Atmospheric Flight Mechanics Conference*, AIAA Paper 2012-4651, Aug. 2012. doi:10.2514/6.2012-4651.

[6] Martos, B., "Identifying and Correcting First Order Effects in Explanatory Variables for Longitudinal Real Time Parameter Identification Methods in Atmospheric Turbulence," Ph.D. thesis, University of Tennessee, Knoxville, Aug. 2013.

[7] Morelli, E., "System IDentification Programs for AirCraft (SIDPAC)," version 4.1, NASA Software Catalog, `http://software.nasa.gov`, accessed Oct. 2019.

[8] McRuer, D., Ashkenas, I., and Graham, D., *Aircraft Dynamics and Automatic Control*, Princeton University Press, Princeton, NJ, 1973, pp. 249–252.

[9] Etkin, B., "Turbulent Wind and Its Effect on Flight," *Journal of Aircraft*, Vol. 18, No. 5, 1981, pp. 327–345. doi:10.2514/3.57498.

[10] Nelson, R., *Flight Stability and Automatic Control*, McGraw-Hill, New York, NY, 1989, pp. 176–197.

[11] Klein, V., "Maximum Likelihood Method for Estimating Airplane Stability and Control Parameters From Flight Data in Frequency Domain," NASA TP-1637, May 1980.

[12] Clementson, G., "An Investigation of the Power Spectral Density of Atmospheric Turbulence," Ph.D. thesis, Massachusetts Institute of Technology, 1950.

[13] Chilton, R., "Some Measurements of Atmospheric Turbulence Obtained from Flow-Direction Vanes Mounted on an Airplane," NACA TN-3313, Nov. 1954.

[14] Notess, C., and Eakin, G., "Flight Test Investigation of Turbulence Spectra at Low Altitude Using a Direct Method for Measuring Gust Velocities," Cornell Aeronautical Laboratory Report No. VC-839-F-1, Jul. 1954.

[15] Grauer, J., "Position Corrections for Airspeed and Flow Angle Measurements on Fixed-Wing Aircraft," NASA TM-2017-219795, Nov. 2017.

[16] Morelli, E., "Real-Time Aerodynamic Parameter Estimation Without Air Flow Angle Measurements," *Journal of Aircraft*, Vol. 49, No. 4, 2012, pp. 1064–1074. doi:10.2514/1.C031568.

[17] Morelli, E., "Dynamic Modeling from Flight Data with Unknown Time Skews," *Journal of Guidance, Control, and Dynamics*, Vol. 40, No. 8, 2017, pp. 2083–2091. doi:10.2514/1.G002008.

[18] Grauer, J., "Random Noise Generation Using Fourier Series," *Journal of Aircraft*, Vol. 55, No. 4, 2018, pp. 1753–1759. doi:10.2514/1.C034616.

[19] Anon., "Flying Qualities of Piloted Aircraft," MIL-STD-1797A, Jan. 1990.

[20] Richardson, J., Atkins, E., Kabamba, P., and Girard, A., "Scaling of Airplane Dynamic Response to Stochastic Gusts," *Journal of Aircraft*, Vol. 51, No. 5, 2014, pp. 1554–1566. doi:10.2514/1.C032410.

[21] Bendat, J., and Piersol, A., *Random Data: Analysis and Measurement Procedures*, 2$^{\text{nd}}$ ed., John Wiley & Sons, Hoboken, NJ, 1986, pp. 130–132.

[22] Grauer, J., Morelli, E., and Murri, D., "Flight-Test Techniques for Quantifying Pitch Rate and Angle-of-Attack Rate Dependencies," *Journal of Aircraft*, Vol. 54, No. 6, 2017, pp. 2367–2377. doi:10.2514/1.C034407.